



Fermi National Accelerator Laboratory

FERMILAB-Conf-95/240-E
CDF

Measurement of the W Boson Mass from CDF

Presented by Y. Kim
For the CDF Collaboration

Fermi National Accelerator Laboratory
P.O. Box 500, Batavia, Illinois 60510

July 1995

Published Proceedings for the *10th Topical Workshop on Proton-Antiproton Collider Physics*,
Fermilab, Batavia, Illinois, May 9-13, 1995

Disclaimer

This report was prepared as an account of work sponsored by an agency of the United States Government. Neither the United States Government nor any agency thereof, nor any of their employees, makes any warranty, expressed or implied, or assumes any legal liability or responsibility for the accuracy, completeness, or usefulness of any information, apparatus, product, or process disclosed, or represents that its use would not infringe privately owned rights. Reference herein to any specific commercial product, process, or service by trade name, trademark, manufacturer, or otherwise, does not necessarily constitute or imply its endorsement, recommendation, or favoring by the United States Government or any agency thereof. The views and opinions of authors expressed herein do not necessarily state or reflect those of the United States Government or any agency thereof.

Measurement of the W Boson Mass from CDF

CDF Collaboration

Presented by Young-Kee Kim

*Lawrence Berkeley Laboratory
Berkeley, CA 94720*

The CDF collaboration has measured the mass of the W boson to be $M_W = 80.41 \pm 0.18$ GeV/ c^2 using 5718 $W \rightarrow e\nu$ events and 3268 $W \rightarrow \mu\nu$ events collected in ~ 19 pb $^{-1}$ from the 1992-93 collider run at the Fermilab Tevatron. This measurement has an uncertainty half that of the best previously published measurements.

I. INTRODUCTION

The relations between gauge boson masses and the couplings of gauge bosons allow incisive tests of the standard model of the electroweak interactions. The relationships are precisely specified at Born level; with higher-order radiative corrections they are sensitive to quark masses, and masses of the W , Z , and Higgs bosons (1). Of these, the top quark mass and the W mass are unique to the Tevatron. A precise measurement of the W mass (M_W), combined with other electroweak precision measurements and the measurement of the top quark mass (M_{top}), tests the consistency of the standard electroweak model, and within the framework of the model, can give an indication of the Higgs mass (M_{Higgs}).

The CDF collaboration has measured the W boson mass using ~ 19 pb $^{-1}$ of data collected between August 1992 and May 1993 (Run Ia) at the Fermilab Tevatron. This document briefly steps through the analysis. The details of the analysis are described in Reference (2).

The W mass is measured by fitting the lineshape of the measured transverse mass (see below) to the lineshapes constructed by Monte Carlo simulation for a range of W masses in both $W \rightarrow e\nu$ and $W \rightarrow \mu\nu$ decays. The transverse mass M_T^W is constructed from the lepton (e or μ) transverse momentum, $\vec{P}_T^{\text{lepton}}$, and the neutrino transverse momentum, \vec{P}_T^ν :

$$M_T^W = \sqrt{2P_T^{\text{lepton}} P_T^\nu (1 - \cos\phi_{\text{lepton},\nu})}$$

with $\phi_{\text{lepton},\nu}$ being the azimuthal angle between the lepton and the neutrino direction. The measurement thus depends critically on the lepton momentum scale and the neutrino momentum scale. The resolution of the lepton and neutrino momentum, as well as the W production process, are also critical.

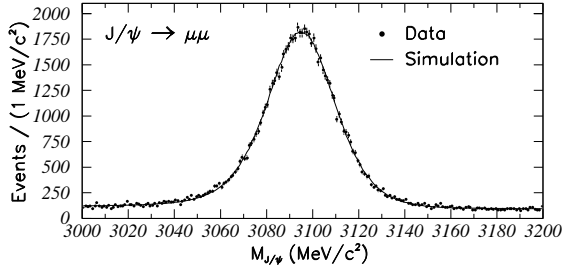


FIG. 1. The dimuon mass spectrum near the J/ψ mass peak, used to normalize the momentum scale. The solid line is the Monte Carlo simulation, including radiative effects.

This paper describes the lepton momentum measurement in section II, the neutrino momentum measurement in section III, the event selection and background in section IV, the physics and detector model in section V, and the fitting procedure in section VI. The systematic uncertainties are discussed in section VII and we present the results in section VIII and future prospects in section IX.

II. LEPTON MOMENTUM MEASUREMENT

The muon momentum is measured from the central tracking chamber (CTC) (3) as it traverses a 1.4 T magnetic field, while the electron energy is measured from the central electromagnetic calorimeter (CEM) (4).

The CTC momentum scale is determined by rescaling the invariant mass of the fitted $J/\psi \rightarrow \mu\mu$ signal to the world average value. We have measured the J/ψ mass to be 3097.3 ± 1.6 MeV as shown in Figure 1 after accounting for energy loss in the detector material, alignment effects, and QED radiation effects. The uncertainty (see Table 1) is dominated by the uncertainty in the muon energy loss due to uncertainty in the material. Normalizing the measured J/ψ mass to the world average value, $M_{J/\psi} = 3096.88 \pm 0.04$ MeV/ c^2 (5), a scale factor of 0.99984 ± 0.00058 is extracted, where the error includes uncertainty in extrapolating from $M_{J/\psi}$ to M_W , and is applied to all the CTC tracks. The scale is verified by measuring the Z and Υ masses (see Figure 2 and Table 2). The uncertainty in the momentum scale contributes 50 MeV/ c^2 to the uncertainty on M_W .

The momentum resolution is determined from the width of the Z mass peak in a sample of 330 $Z \rightarrow \mu\mu$ events in the range $76 < M_{\mu\mu} < 106$ GeV/ c^2 . It is measured to be $\delta p_T/p_T^2 = 0.000810 \pm 0.000085(\text{stat.}) \pm 0.000010(\text{syst.})$ (GeV/ c) $^{-1}$, and the uncertainty on the resolution contributes 60 MeV/ c^2 to the uncertainty on M_W .

The CEM energy scale is determined by fitting the E/p lineshape of elec-

Effect	Uncertainty (MeV/c ²)
Statistics	0.1
Background	0.1
Muon energy loss before tracking	1.3
Beam constraint, Residual field non-uniformity, Time variation	0.8
Radiative decay	0.2
SUBTOTAL	1.6
Extrapolation from $M_{J/\psi}$ to M_W	0.9
TOTAL	1.8

TABLE 1. Uncertainties on using the J/ψ mass to set the momentum scale for electrons and muons from W decays, expressed as the uncertainty on the J/ψ mass in MeV/c². The tabulation includes the uncertainty incurred when extrapolating from tracks in J/ψ decays to tracks with zero curvature.

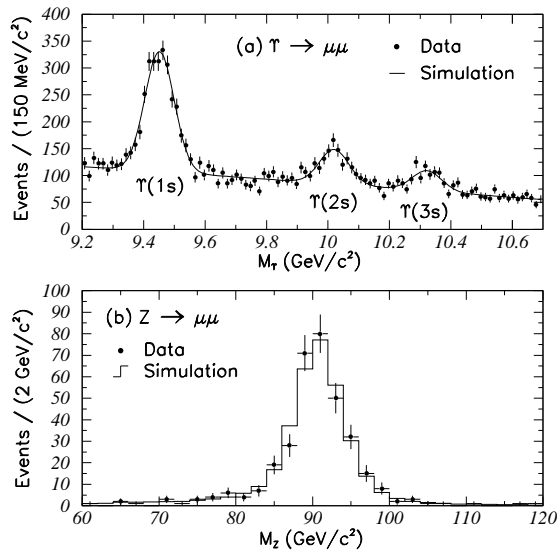


FIG. 2. (a) The dimuon mass spectrum near the Υ mass peaks, used to check the momentum scale. (b) The dimuon mass spectrum near the Z mass peak, used to check the momentum scale and to determine the momentum resolution. The histogram is the Monte Carlo simulation, including radiative effects.

Resonance	Corrected Mass (MeV/c ²)	World-Average Mass (MeV/c ²)
$\Upsilon(1S) \rightarrow \mu\mu$	$9460 \pm 2 \pm 6$	9460.4 ± 0.2
$\Upsilon(2S) \rightarrow \mu\mu$	$10029 \pm 5 \pm 6$	10023.3 ± 0.3
$\Upsilon(3S) \rightarrow \mu\mu$	$10334 \pm 8 \pm 6$	10355.3 ± 0.5
$Z \rightarrow \mu\mu$	$91020 \pm 210 \pm 55 \pm 40$	91187 ± 7
$Z \rightarrow ee$	$90880 \pm 185 \pm 135 \pm 150$	91187 ± 7

TABLE 2. Measured masses of the $\Upsilon \rightarrow \mu\mu$, $Z \rightarrow \mu\mu$, and $Z \rightarrow ee$ resonances compared to the published values (5). The first, second, and third uncertainties on the corrected value are from statistics, the momentum scale, and the other systematics, respectively.

trons from W decays to a simulated lineshape, where E is the CEM measurement of energy and p is the CTC measurement of the track momentum. Before the scale is determined, the CEM response is equalized as a function of the electron impact point using E/p for electrons in a sample of $\sim 140,000$ events with $E_T > 9$ GeV, resulting in better resolution for the electron energy. The E/p distribution for the W electrons after this correction is shown in Figure 3 (a). The long tail on the right-hand side of the distribution is due to internal bremsstrahlung, and external bremsstrahlung before entering the tracking volume and in the tracking volume. Since the photon is nearly collinear with the electron, E is largely unaffected by the bremsstrahlung but p is lowered, resulting in the long tail. The solid histogram is from a radiative Monte Carlo which includes the contributions from both internal and external radiation of photons. The CEM scale determined from the peak region ($0.9 < E/p < 1.1$) provides a statistical precision of 0.08% and a systematic uncertainty of 0.11%, corresponding to uncertainties of 65 MeV/c² and 90 MeV/c² on M_W (see Table 3). The systematic uncertainty is dominated by uncertainty in the detector material which is measured by the ratio of the number of events in the tail ($1.3 < E/p < 2.0$) to the number of events in the peak ($0.8 < E/p < 1.2$). The total energy scale uncertainty including the momentum scale uncertainty of 50 MeV/c² is 120 MeV/c². The energy scale is verified by measuring the $Z \rightarrow ee$ mass in a sample of 259 $Z \rightarrow ee$ events in the range $81 < M_{ee} < 101$ GeV/c² where both electrons are in the CEM (see Figure 3 (b) and Table 2).

The energy resolution is determined from the width of the $Z \rightarrow ee$ mass peak. It is measured to be $(\delta E/E)^2 = (13.5\%/\sqrt{E_T})^2 + (1.0 \pm 1.0\%)^2$, and the uncertainty of the resolution leads to an uncertainty of 80 MeV/c² on M_W .

III. NEUTRINO MOMENTUM MEASUREMENT

The neutrino transverse momentum is inferred from the lepton momentum described in the previous section and the W transverse momentum which is

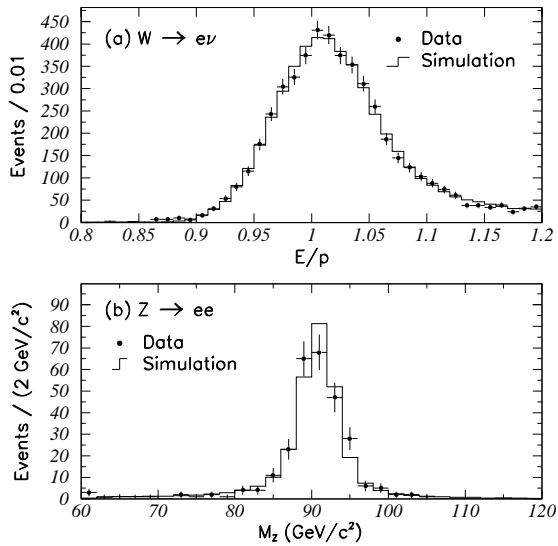


FIG. 3. (a) The E/p spectrum for electrons from the $W \rightarrow e\nu$ sample, used to determine the energy scale. (b) The dielectron mass spectrum near the Z mass peak, used to check the energy scale and to determine the energy resolution. The histograms are Monte Carlo simulations, including radiative effects.

Source of Uncertainty	Uncertainty in $M_{W^e}^e$ (MeV/c ²)
Statistics	65
External bremsstrahlung (Material)	70
Electron resolution	50
Fitting	15
Total	110

TABLE 3. Uncertainties incurred setting the energy scale from the momentum scale.

described in this section. The W transverse momentum is measured by the calorimeter energy (recoil energy, \vec{u}) from the hadrons which recoil against the W , and from the underlying event. We first separate lepton energy from the recoil energy by removing the calorimeter towers associated with the lepton and replacing it with average underlying event E_T , 30 ± 3 MeV per tower. We then calculate \vec{u} by summing all the calorimeter E_T in vector,

$$\vec{u} = \sum_{\text{towers}} E^{\text{tower}} (\hat{n} \cdot \hat{r})$$

where E^{tower} is the energy measured in the electromagnetic or hadronic calorimeter tower, \hat{n} is the unit vector pointing in the direction of the center of the tower from the event vertex, and \hat{r} is the unit vector in the radial direction (2). The sum is carried out for towers in the region $|\eta| < 3.6$. The missing momentum, thus the neutrino momentum, is reconstructed from the transverse energy balance

$$\vec{P}_T^\nu = -\vec{P}_T^{\text{lepton}} - \vec{u}.$$

\vec{u} is a rather poor measurement: the averaged response $\langle |\vec{u}| \rangle$ is smaller than $\langle p_T^W \rangle$ since energies of recoiling hadrons are low where calorimeter response is not linear, and its resolution is poor because of the underlying event. No correction is made to \vec{u} . Instead we model the detector response of \vec{u} in the simulation, which is described in section V.

IV. EVENT SELECTION AND BACKGROUND

The event selection is intended to produce a sample of W bosons with low background and well-understood lepton and neutrino kinematics. Electrons are required to be within a restricted fiducial region of the CEM and have $E_T^e > 25$ GeV. Muons are required to be within the fiducial region of the CMU and to have $p_T^\mu > 25$ GeV/c. Neutrinos are required to have $E_T^\nu > 25$ GeV. In addition we require $|\vec{u}| < 20$ GeV, no jet with $E_T > 30$ GeV, and no tracks with $p_T > 10$ GeV/c other than that of the charged lepton. Events consistent with cosmic rays or $Z \rightarrow ll$ are removed. The lepton track is required to come from an event vertex located within 60 cm of the detector center along the z axis. The $W \rightarrow \mu\nu$ sample consists of 3268 events with transverse masses in the range $65 < M_T < 100$ GeV/ c^2 ; the $W \rightarrow e\nu$ sample consists of 5718 events in the same M_T range.

We estimate the background from the process $W \rightarrow \tau\nu \rightarrow l\nu\nu\nu$ to be 0.8% of the $W \rightarrow e\nu$ and $W \rightarrow \mu\nu$ samples. Events from $Z \rightarrow ll$ where one lepton is lost make up 0.1% of the $W \rightarrow e\nu$ sample, and $(3.6 \pm 0.5)\%$ of the $W \rightarrow \mu\nu$ sample. The $Z \rightarrow \mu\mu$ background in the $W \rightarrow \mu\nu$ sample is large because neither the CTC nor the muon chambers cover the high η region. Backgrounds from $W \rightarrow \tau\nu \rightarrow h + X$, where h is a single charged hadron, $Z \rightarrow \tau\tau$, WW and $t\bar{t}$ production, and cosmic rays are estimated to be small. Transverse mass spectra of the backgrounds are shown in Figure 4.

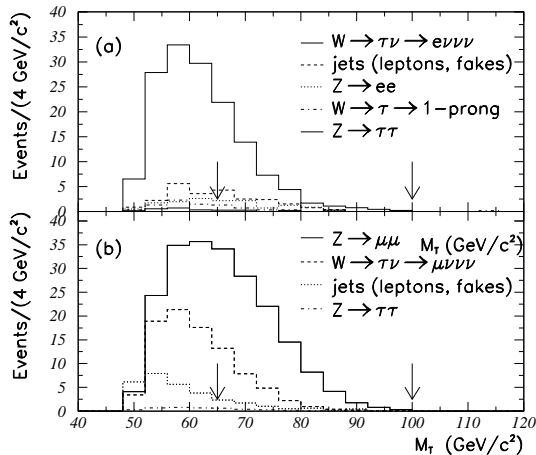


FIG. 4. The M_T^W distributions of the backgrounds in (a) the $W \rightarrow e\nu$ sample and (b) the $W \rightarrow \mu\nu$ sample. The arrows delimit the fitting region.

V. PHYSICS AND DETECTOR MODEL

W events are generated with a leading-order calculation (*i.e.* $p_T^W=0$) using the MRS D'_- parton distribution functions. We incorporate a p_T^W spectrum using the observed $Z \rightarrow ee$ p_T spectrum, lead by the similarity of the p_T spectra of W and Z bosons (6). The $Z \rightarrow ee$ p_T spectrum is corrected for electron energy resolutions and modified until the observed u_\perp distribution for the W events matches with the simulated distribution, where u_\perp is the component of the recoil \vec{u} perpendicular to the direction of the charged lepton. We find that the simplest modification, scaling p_T in the p_T^Z distribution by a constant factor of ~ 1.1 , gives good agreement for both electron and muon u_\perp distributions. The W then decays into a lepton and a neutrino.

The momentum and energy resolutions of leptons are incorporated in the simulation. The detector response to the recoil energy \vec{u} is directly modeled using $Z \rightarrow ee$ decays, for which there is a good measurement of the true p_T^Z from the measured electron energies. A sample of 555 $Z \rightarrow ee$ events, where one of the electrons is in the CEM and the other is in $|\eta| < \sim 4$, is used as a table from which one can look up the measured response \vec{u} for a given p_T^Z . We assume that the response to the recoil from a W of a given p_T is the same as that to the recoil from a Z of the same p_T .

The value of u_\parallel , the component of \vec{u} parallel to the charged lepton direction, contains most of the transverse mass information and it is the quantity sensitive to the lepton selection criteria, the residual leakage of the lepton energy, and the energy deposited under the lepton by the underlying event. Figure 5 shows that u_\parallel in the data is well modeled by the simulation over the full range of P_T^{lepton} . Similar agreement is seen over the full range of P_T^ν and M_T^W .

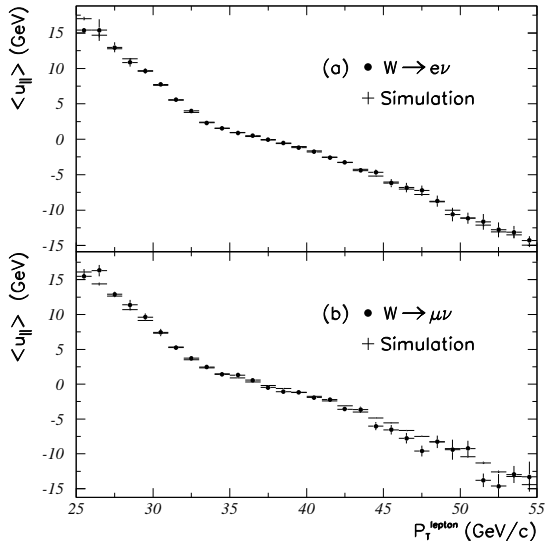


FIG. 5. The $\langle u_{\parallel} \rangle$ as a function of the lepton P_T for (a) the $W \rightarrow e\nu$ decay and (b) the $W \rightarrow \mu\nu$ decay. for the data and the simulation.

VI. FITTING PROCEDURE

Transverse mass spectra are generated for a range of W masses, at $100 \text{ MeV}/c^2$ intervals for $W \rightarrow e\nu$, and $150 \text{ MeV}/c^2$ intervals for $W \rightarrow \mu\nu$. At each mass point, an unbinned log-likelihood is calculated. The W mass is determined by fitting the log-likelihood values to a parabola.

VII. SYSTEMATIC UNCERTAINTIES AND CORRECTIONS

The individual uncertainties and corrections in the W mass measurement are briefly described, followed by a summary of the systematic uncertainties.

Lepton Momentum Scale: The uncertainty on the muon momentum scale comes from the CTC scale and is 50 MeV as explained in section II. For the electrons, in addition to the CTC scale uncertainty, there is a 110 MeV uncertainty on the CEM scale from the E/p lineshape fitting procedure. The total uncertainty for electrons is then 120 MeV .

Lepton Momentum Resolution: Uncertainties of the electron and muon momentum resolutions extracted from the $Z \rightarrow ee$ and $Z \rightarrow \mu\mu$ widths (see section II) lead to uncertainties of 80 MeV and 60 MeV on M_W , respectively.

Recoil Modeling: Uncertainties in the recoil modeling are incurred from using the $Z \rightarrow ee$ events to calibrate the detector response to the W recoil.

Two effects are investigated: statistical fluctuations arising from the finite size of the Z sample, leading to an uncertainty of $50 \text{ MeV}/c^2$ on M_W , and the effect of electron energy resolution on the p_T^Z measurement, leading to an uncertainty of $35 \text{ MeV}/c^2$ on M_W . The uncertainties are common to the $W \rightarrow e\nu$ and $W \rightarrow \mu\nu$ channels.

Lepton Identification and Removal: Efficiency of identifying leptons may decrease as the leptons get close to the direction of the recoiling hadrons, which may result in a bias on $u_{||}$. Any residual leakage from the lepton energy into surrounding calorimeter towers or errors in accounting for the energy deposited under the lepton by the underlying event will also induce a bias on $u_{||}$. The combination of these effects contributes an uncertainty of $25 \text{ MeV}/c^2$ on M_W in the $W \rightarrow e\nu$ channel, and $10 \text{ MeV}/c^2$ on M_W in the $W \rightarrow \mu\nu$ channel, of which $5 \text{ MeV}/c^2$, due to the lepton removal, is common.

Trigger Bias: The triggers for the $W \rightarrow l\nu$ sample may affect the W mass measurement if there is a kinematic (for example, P_T^{lepton}) dependence upon the efficiency. The trigger bias in the $W \rightarrow e\nu$ sample is negligible since there are redundant triggers providing the sample. The $W \rightarrow \mu\nu$ sample is provided by only the tracking trigger. No p_T^μ -dependence is seen, but the statistical limitation on measuring such a dependence leads to a $25 \text{ MeV}/c^2$ uncertainty on the $W \rightarrow \mu\nu$ mass.

Backgrounds: Backgrounds shown in Figure 4 are directly included in the simulated lineshapes, with the exception of small backgrounds in the muon channel from $Z \rightarrow \tau\tau$ and jet or heavy-flavor production. The total effect of backgrounds on the measured W mass is $60 \text{ MeV}/c^2$ in the electron channel and $197 \text{ MeV}/c^2$ in the muon channel. The uncertainties are $10 \text{ MeV}/c^2$ and $25 \text{ MeV}/c^2$ in the electron and muon channel, respectively.

p_T^W Distributions: The systematic effects due to the p_T^W distributions were investigated by varying the input p_T^W distribution. An uncertainty of $45 \text{ MeV}/c^2$ on M_W is estimated, of which $25 \text{ MeV}/c^2$ is common to the $W \rightarrow e\nu$ and $W \rightarrow \mu\nu$ analyses.

p_Z^W Distributions (Parton Distribution Functions): Varying the parton distribution functions (PDFs) of the proton varies the distribution of the W longitudinal momentum (p_Z^W), and, through acceptance effects, the lineshape of the transverse mass spectrum. The CDF measurement of the forward-backward charge asymmetry in W decay (7) is used to constrain p_Z^W . Figure 6 shows the change in derived $W \rightarrow e\nu, \mu\nu$ mass ($\Delta M_W^{e,\mu}$) versus the signed deviation from the average W asymmetry measurement (ζ) in units of the standard deviation for various PDFs (8). By allowing $\pm 2\sigma$ deviation in the asymmetry (see Figure 6), we determine the uncertainty due to the choice of PDF to be $50 \text{ MeV}/c^2$ for the both $W \rightarrow e\nu$ and $W \rightarrow \mu\nu$ channels.

QCD higher-order Corrections: The physics simulations use a Born-level matrix element calculation for W production, augmented by a realistic p_T^W

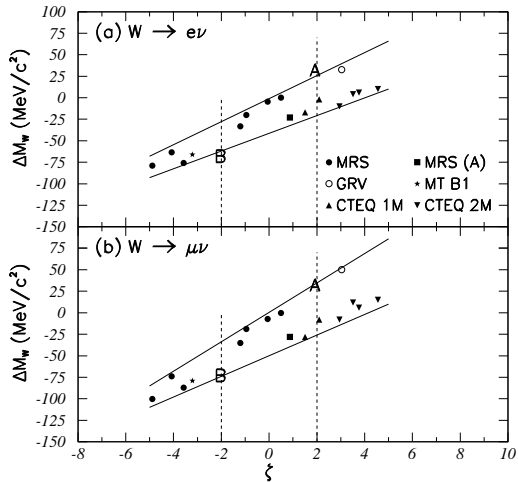


FIG. 6. Change in derived W mass (ΔM_W) versus the signed deviation from the average W asymmetry measurement (ζ) in units of the standard deviation for various PDFs, for the (a) $W \rightarrow e\nu$ and (b) $W \rightarrow \mu\nu$ decays.

distribution. The true production mechanisms (even at low p_T^W) include additional higher-order QCD corrections. These corrections will affect p_Z^W , as well as the polarization of the produced W . No measurable shift of the W mass due to these effects is observed. The ability to measure such a shift, 20 MeV/c², is taken as an uncertainty for both the $W \rightarrow e\nu$ and $W \rightarrow \mu\nu$ analyses, of which 10 MeV/c² is from effects in the W polarization and 15 MeV/c² is from effects in the W longitudinal momentum.

Radiative Correction: The W mass shift due to radiative W decays, $W \rightarrow e\nu\gamma$ and $W \rightarrow \mu\nu\gamma$, is determined by using an $O(\alpha)$ Monte Carlo program (9). Collinear photons, landing in the calorimeter towers traversed by leptons, are lost for the muon channel and are included in the electron energy for the electron channel. Photons, isolated from leptons, are included in the calculation of \vec{u} . We add 65 and 168 MeV/c² to the fitted masses in the electron and muon channels, respectively, to account for the effects of radiative W decay. The uncertainty in the theoretical calculation used and the photon simulation leads to 20 MeV/c² uncertainty on M_W , which is common to the $W \rightarrow e\nu$ and $W \rightarrow \mu\nu$ decays.

W Width: The value of the W width used in the simulation is the measured value of 2.064 ± 0.085 GeV/c² (10). The uncertainty on the W width leads to an uncertainty of 20 MeV/c² on M_W , which is common to the $W \rightarrow e\nu$ and $W \rightarrow \mu\nu$ decays.

Fitting Procedure: A 10 MeV/c² uncertainty on M_W , independent in the electron and muon analyses, is taken due to the finite statistics used to gen-

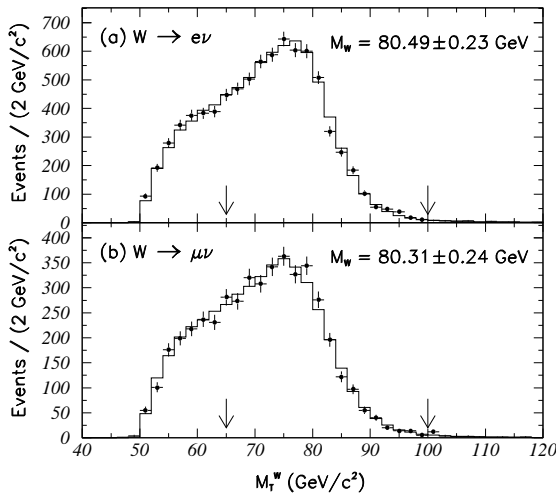


FIG. 7. Transverse mass spectra for (a) $W \rightarrow e\nu$ decays and (b) $W \rightarrow \mu\nu$ decays. The histograms are from the simulation using the respective best-fit mass. The arrows delimit the region used in the mass fit.

erate the transverse mass lineshapes.

VIII. RESULTS

We obtain the W mass of

$$M_W^e = 80.490 \pm 0.145(\text{stat.}) \pm 0.175(\text{syst.}) \text{ GeV}/c^2,$$

using the $W \rightarrow e\nu$ decays, and

$$M_W^\mu = 80.310 \pm 0.205(\text{stat.}) \pm 0.130(\text{syst.}) \text{ GeV}/c^2,$$

using the $W \rightarrow \mu\nu$ decays, where the W width is fixed at 2.06 GeV. The transverse mass spectra and the Monte Carlo lineshapes corresponding to the best fit mass are shown in Figure 7. Accounting for correlations in the uncertainties, the combined data yield

$$M_W = 80.41 \pm 0.18 \text{ GeV}/c^2.$$

Fits in which the W width is allowed to vary, as well as fits to the P_T^{lepton} distributions and to the P_T^ν distributions give consistent results (2). In Figure 8, we compare this measurement to other measurements by the CDF (11), UA2 (12) and D0 (13) experiments. The present CDF measurement has an uncertainty half that of the best previously published measurements (11,12). Combining these W mass measurements, assuming a common error of 85 MeV/ c^2 for the parton distribution functions, gives

$$M_W = 80.25 \pm 0.16 \text{ GeV}/c^2,$$

Source of Uncertainty	Uncertainty (MeV/c ²)		
	$W \rightarrow e\nu$	$W \rightarrow \mu\nu$	Common
Statistical	145	205	–
Energy Scale	120	50	50
Scale from J/ψ	50	50	50
CTC Alignment	15	15	15
Calorimeter	110	–	–
Stat. on E/p	65		
Syst. on E/p	90		
Other Systematics	130	120	90
e or μ resolution	80	60	–
Recoil energy modeling	60	60	60
e or μ ID and removal	25	10	5
Trigger bias	0	25	–
Backgrounds	10	25	–
p_T^W	45	45	25
p_Z^W (Parton dist. functions)	50	50	50
QCD Higher-order corrections	20	20	20
QED Radiative corrections	20	20	20
W width	20	20	20
Fitting procedure	10	10	–
TOTAL UNCERTAINTY	230	240	100

TABLE 4. Summary of uncertainties in the W mass measurement.

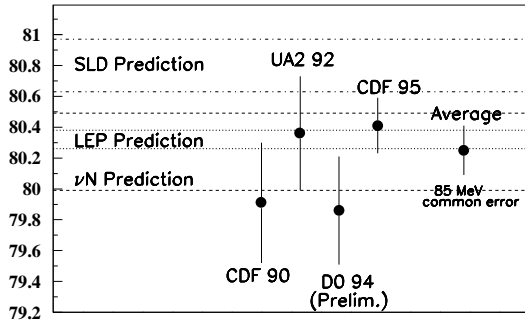


FIG. 8. The current measurement of the W mass is compared to measurements from previous or other experiments.

dominated by the CDF measurement. These are in a good agreement with the LEP prediction (14) for the W mass (see Figure 8). Figure 9 shows the sensitivity in the M_W - M_{top} plane of this CDF result, $M_W = 80.41 \pm 0.18 \text{ GeV}/c^2$, when combined with the top mass of $M_{\text{top}} = 176 \pm 13 \text{ GeV}/c^2$ (15), compared to theoretical predictions based on electroweak radiative corrections (16).

IX. FUTURE PROSPECTS

We have been collecting additional data (Run Ib) since November 1993, and expect to acquire a factor of five the present analysis by July 1995 as illustrated in Figure 10. The uncertainties in the current measurement scale rather well in detail from the previous measurement; while the difficulty of the measurement has increased, no systematic limitation is yet evident. A dominant uncertainty in the momentum and energy scale is from the uncertainty in the detector material. We have recently found that photon conversions allow us to measure the amount of material much better than the method we used for the current measurement, as illustrated in Figures 11 and 12, and can reduce the uncertainties on the W mass measurement. The uncertainty due to the PDF choice will be reduced by using better measurement of the W charge asymmetry (17). Most of the other systematic errors will also be reduced since they are limited by the statistics of W 's and Z 's. We expect to measure the W mass better than $100 \text{ MeV}/c^2$ for Run Ib.

For 2 fb^{-1} of data with the Main Injector (Run II), we estimate an error of approximately $40 \text{ MeV}/c^2$ which is dominated by theoretical uncertainties associated with the details of the production process, for instance, the parton distribution functions. The error is certainly comparable to the overall LEP-200 expectation. Figure 12 shows the sensitivity in the M_W - M_{top} plane of this estimate when combined with the estimate of δM_{top} for 2 fb^{-1} of data.

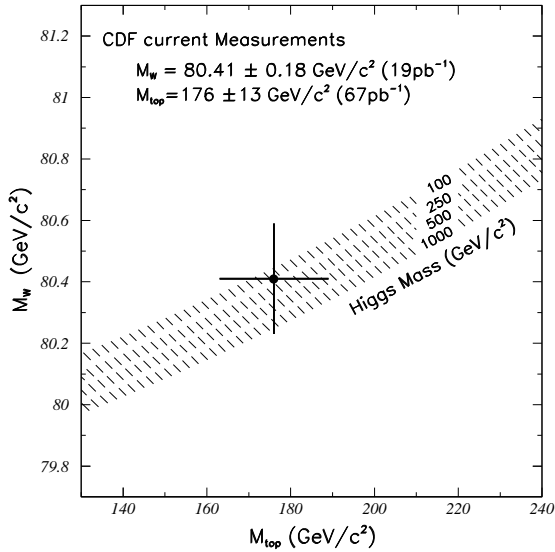


FIG. 9. The data point represents the CDF measurements of M_W and M_{top} . The curves are from a calculation (16) of the dependence of M_W on M_{top} in the minimal standard model using several Higgs masses. The bands are the uncertainties obtained by folding in quadrature uncertainties on $\alpha(M_Z^2)$, M_Z , and $\alpha_s(M_Z^2)$.

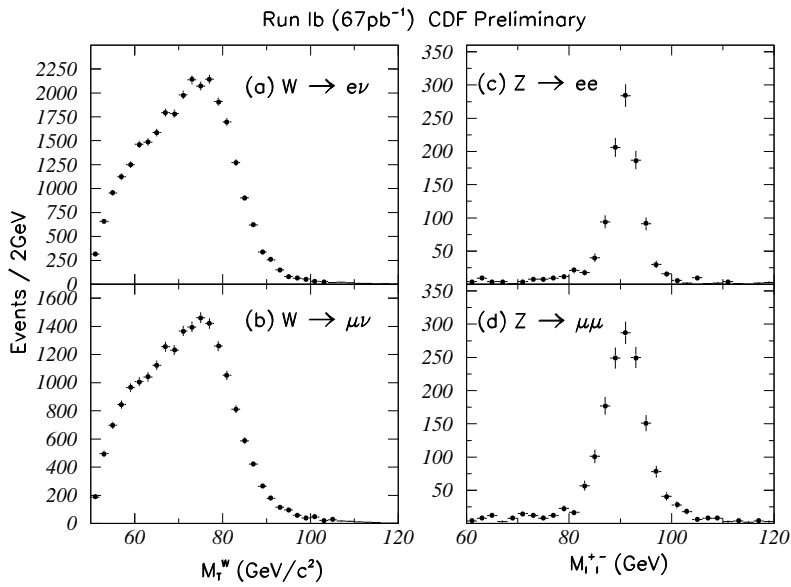


FIG. 10. Transverse mass spectra for (a) $W \rightarrow e\nu$ and (b) $W \rightarrow \mu\nu$ decays, and invariant mass spectra for (c) $Z \rightarrow ee$ and (d) $Z \rightarrow \mu\mu$ decays, for $\sim 67 \text{ pb}^{-1}$ of Run Ib data.

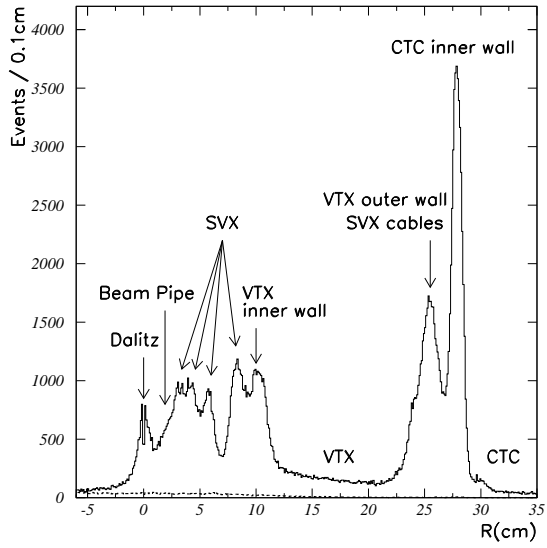


FIG. 11. The radial distributions for photon conversions (solid line) and background (dashed line).

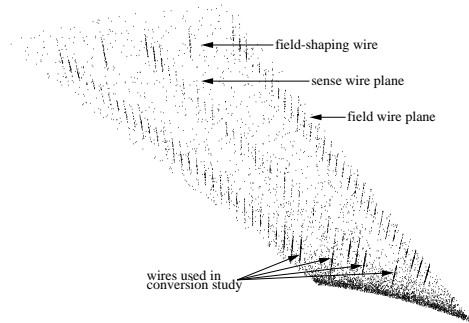


FIG. 12. Reconstructed photon conversion vertex density in the r - ϕ plane for the innermost super-layer in the CTC, folded into $1/30$ of the circumference (this layer has 30-fold symmetry).

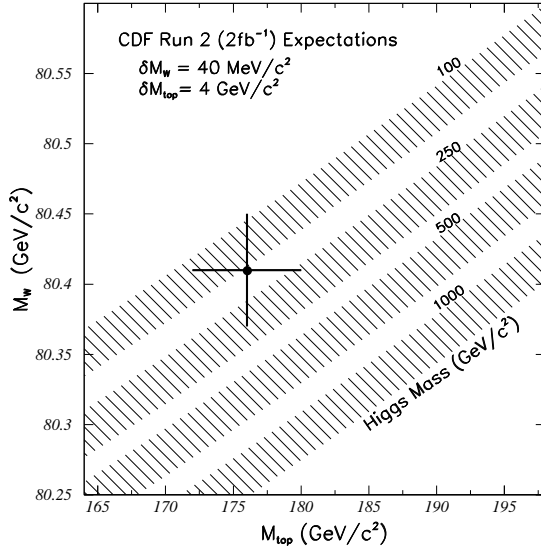


FIG. 13. The data point represents the CDF estimate of M_W and M_{top} for 2 fb^{-1} of data. Note that the scale is different from Figure 9.

ACKNOWLEDGEMENT

We thank the Fermilab staff and the technical staffs of the participating institutions for their contributions. This work was supported by the U.S. Department of Energy and National Science Foundation; the Italian Istituto Nazionale di Fisica Nucleare; the Ministry of Science, Culture, and Education of Japan; the Natural Sciences and Engineering Research Council of Canada; the A. P. Sloan Foundation; and the Grainger Foundation.

REFERENCES

1. For recent reviews, see W. Hollik and W. Marciano, in "Precision Tests of the Standard Electroweak Model", ed. by P. Langacker (World Scientific, Singapore, 1994), and B. A. Kniehl, KEK preprint KEK-TH-412, Sept. 1994, submitted to Int. J. Mod. Phys. A.
2. F. Abe *et al.* (CDF Collaboration), Fermilab preprint FERMILAB-PUB-95/033-E (1995), submitted to Phys. Rev. D.; F. Abe *et al.* (CDF Collaboration), Phys. Rev. Lett., **75**, 11 (1995).
3. F. Bedeschi *et al.*, Nucl. Instrum. Methods, **A268**, 50 (1988).
4. L. Balka *et al.*, Nucl. Instrum. Methods, **A267**, 272 (1988); S. R. Hahn *et al.*, Nucl. Instrum. Methods, **A267**, 351 (1988); K. Yasuoka *et al.*, Nucl. Instrum.

- Methods, **A267**, 315 (1988); R. G. Wagner *et al.*, Nucl. Instrum. Methods, **A267**, 330 (1988); T. Devlin *et al.*, Nucl. Instrum. Methods, **A267**, 24 (1988).
5. L. Montanet *et al.* (PDG), *Review of Particle Properties*, Phys. Rev., **D50**, (1994).
 6. F. Abe *et al.* (CDF Collaboration), Phys. Rev. Lett., **66**, 2951 (1991); F. Abe *et al.* (CDF Collaboration), Phys. Rev. Lett., **67**, 2937 (1991). M. H. Reno, University of Iowa preprint UIOWA-94-01, 1994.
 7. F. Abe *et al.* (CDF Collaboration), Phys. Rev. Lett., **74**, 850 (1995).
 8. A.D. Martin, R.G. Roberts and W.J. Stirling, RAL-92-099 (1993).
 9. F. A. Berends and R. Kleiss, Z. Phys., **C27**, 365 (1985). The calculations are implemented in a Monte Carlo program described in R. G. Wagner, Comput. Phys. Commun., **70**, 15 (1992).
 10. F. Abe *et al.* (CDF Collaboration), Phys. Rev. Lett., **73**, 220 (1994).
 11. F. Abe *et al.* (CDF Collaboration), Phys. Rev. Lett., **62**, 1005 (1989).
 12. J. Alitti *et al.* (UA2 Collaboration), Phys. Lett., **B241**, 150 (1990).
 13. Q. Zhu (D0 Collaboration) at "The Ninth Topical Workshop on Proton-Antiproton Collider Physics", Oct. 18-22, 1993.
 14. Talk by D. Schaile in these proceedings.
 15. F. Abe *et al.*, Fermilab preprint FERMILAB-PUB-95/022-E, submitted to Phys. Rev. Lett.
 16. The curves are calculated using a FORTRAN program from F. Halzen and B.A. Kniehl (private communication), described in Nucl. Phys. **B353**, 567 (1990). See Ref. 4 for details.
 17. Talk by P. DeBarbaro in these proceedings.